



# Time-dependent motion of a confined bubble in a tube: transition between two steady states

Yingxian Estella Yu<sup>1</sup>, Lailai Zhu<sup>1,2</sup>, Suin Shim<sup>1</sup>, Jens Eggers<sup>3,†</sup>  
and Howard A. Stone<sup>1,†</sup>

<sup>1</sup>Department of Mechanical and Aerospace Engineering, Princeton University, Princeton, NJ 08544, USA

<sup>2</sup>Linné Flow Centre and Swedish e-Science Research Centre (SeRC), KTH Mechanics, SE 10044 Stockholm, Sweden

<sup>3</sup>School of Mathematics, University of Bristol, University Walk, Bristol BS8 1TW, UK

(Received 8 August 2018; revised 11 October 2018; accepted 11 October 2018)

When a confined bubble translates steadily in a cylindrical capillary tube, without the consideration of gravity effects, a uniform thin film of liquid separates the bubble surface and the tube wall. In this work, we investigate how this steady state is established by considering the transitional motion of the bubble as it adjusts its film thickness profile between two steady states, characterized by two different bubble speeds. During the transition, two uniform film regions coexist, separated by a step-like transitional region. The transitional motion also requires modification of the film solution near the rear of the bubble, which depends on the ratio of the two capillary numbers. These theoretical results are verified by experiments and numerical simulations.

**Key words:** bubble dynamics, lubrication theory, thin films

## 1. Introduction

The motion of elongated bubbles confined in small geometries is of significant geological, industrial and medical interests. Examples include enhanced oil recovery (Blunt 2001), coating processes (Quérel 1999; Stone 2010; Kotula & Anna 2012), particle separation (Yu, Khodaparast & Stone 2018) and lung biomechanics (Gaver *et al.* 1996; Hazel & Heil 2003). When a bubble of length  $L > 2R$  translates steadily in a circular capillary of radius  $R$ , a thin film of liquid separates the bubble surface and the tube wall, as first observed by Fairbrother & Stubbs (1935). The thickness of this lubricating film is of particular interest, since it is crucial to the mass and heat transfer in this multiphase hydrodynamic configuration. The relationship between the

† Email addresses for correspondence: [jens.eggerts@bris.ac.uk](mailto:jens.eggerts@bris.ac.uk), [hastone@princeton.edu](mailto:hastone@princeton.edu)

film thickness and the bubble velocity  $U$  was investigated theoretically by Bretherton (1961) and experimentally by Taylor (1961). Bretherton (1961) found that, with negligible buoyancy and inertial effects, the lubricating film is uniform near the centre of a long bubble, and the film thickness  $h^\infty$  is given by

$$h^\infty/R = 0.643(3Ca)^{2/3}, \quad (1.1)$$

where the capillary number  $Ca \equiv \mu U/\gamma$  is the dimensionless speed of the bubble, and  $\mu$  and  $\gamma$  represent the fluid viscosity and surface tension, respectively.

The dynamics of a long, confined bubble in a circular capillary has been widely investigated thereafter, including effects from finite capillary numbers, inertia, liquid impurities, buoyancy, etc. For example, the uniform film thickness increases with an increase in the bubble velocity, in which case finite capillary numbers and inertia become significant (e.g. Aussillous & Quéré 2000; Heil 2001; de Ryck 2002; Khodaparast *et al.* 2015; Magnini *et al.* 2017). Aussillous & Quéré (2000), for instance, provided a scaling argument to extend (1.1) to a larger range of  $Ca$  and fitted the experimental results from Taylor (1961). Several accounts have been carried out considering the effects of impurities in the continuous fluid phase, including surfactants and suspensions. While both impurities thicken the film, surfactants increase the film thickness by introducing additional fluid flux due to a Marangoni stress (Ratulowski & Chang 1990; Park 1992; Stebe & Barthes-Biesel 1995; Olgac & Muradoglu 2013), and suspensions, which lead to particles being adsorbed on the interface, thicken the film by modifying the boundary condition on the bubble surface (Yu, Khodaparast & Stone 2017). Moreover, as the tube radius  $R$  increases, buoyancy effects can become significant, which can break the film thickness uniformity or lead to film rupture (Leung *et al.* 2012; Atasi *et al.* 2017; Lamstaes & Eggers 2017).

Although a wide variety of investigations have been carried out analysing the relationship between the film profile and the bubble velocity, most of the literature considers the case where the translational velocity is a constant, thus the bubble profile is steady. Instead, in this paper, we ask how such a steady state is established. In order to start from a well-defined initial condition, we investigate the time-dependent dynamics of a bubble as it transits from one steady state at  $Ca_1$  to another steady state at  $Ca_2$ , as shown in figure 1(a). We consider the bubble translation in pure liquid, neglecting inertial and buoyancy effects, such that the film thickness at each steady state is governed by the corresponding  $Ca$ , and thus can be predicted by Bretherton's result (1961), or Aussillous and Quéré's correlation (2000) at higher  $Ca$ . Different film regions are categorized in § 2, where the theoretical derivation of the time-dependent profile will be given. The experimental setup and numerical methods are described in § 3, followed by the results and a comparison among theoretical, experimental and numerical results in § 4.

## 2. Theoretical derivation

The structure of the transitional film profile solution is shown in figure 1(b). The front of the bubble (region I) moves at the new speed  $U_2$ . In the lubrication limit, a film of thickness  $h_2^\infty$  is selected according to (1.1), and a uniform film of this thickness is formed. Since there is no horizontal pressure gradient along the uniform film region, there is no motion in the film relative to the tube wall. In the rear part of the bubble (region IV), the film still has its thickness  $h_1^\infty$  corresponding to the initial speed  $U_1$ . The two film regions are separated by a step (region III), which remains stationary in the frame of the tube, as we will show below. Thus the length

*Time-dependent motion of a confined bubble in a tube*

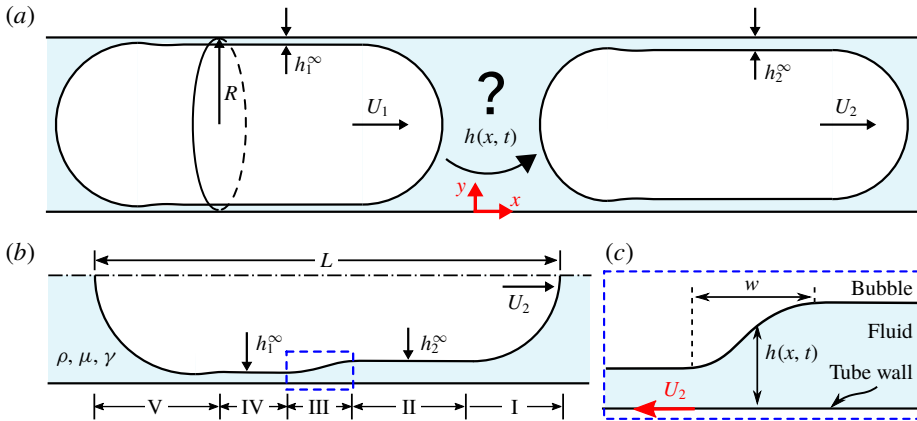


FIGURE 1. Schematics of a bubble translating in a circular capillary between two steady states. (a) Problem statement. The transitional dynamics and film profile  $h(x, t)$  are obtained as a bubble transits between two steady-state speeds from  $U_1$  and  $U_2$ , where it develops the corresponding films of uniform thicknesses  $h_1^\infty$  and  $h_2^\infty$ . An  $(x, y)$  coordinate system can be used to describe the film profile for this axisymmetric problem. (b) Schematic of the transitional bubble film profile, where five regions are categorized. (c) Schematic of the step-like transitional region.

of region II is determined by how much the front of the bubble has advanced since the change in speed at  $t=0$ , which is  $L_{II} \approx U_2 t$ . Finally, there is a thin film region in the back of the bubble that exhibits the characteristic oscillations found by Bretherton (1961). However, owing to the incompressibility, the rear of the bubble moves at the same speed as the front, producing a mismatch between the speed  $U_2$  and the film thickness  $h_1^\infty$ . As a result, the shape of the film at the back differs from that found for the classical steady-state Bretherton problem.

*2.1. Uniform film thickness at steady state*

We begin by summarizing Bretherton’s original steady solution, which describes the steady states shown in figure 1(a) and forms the basis for our description during the transition. The bubble surface is separated from the inner tube wall by a uniform thin liquid film of thickness  $h^\infty$ . Since the film thickness is much smaller than  $R$ , we can describe the film motion in an  $(x, y)$  coordinate system as shown in figure 1(a). In the limit of small capillary numbers, it follows that  $|dh/dx| \ll 1$  (as we confirm below), and the dynamics of the film are described by the lubrication equation (Eggers & Fontelos 2015)

$$h_t + \frac{\gamma}{3\mu} (h^3 h_{xxx})_x = 0, \tag{2.1}$$

which describes the viscous motion inside the film in response to the gradient of the capillary pressure  $-\gamma h_{xx}$  (here subscripts denote derivatives). Moving with the bubble at the steady-state velocity  $U$ , the solution is of the form  $h(x, t) = h(x - Ut)$ . Combining with (2.1) and integrating once over  $x$ , we obtain

$$h^3 h_{xxx} + 3Ca(h^\infty - h) = 0. \tag{2.2}$$

Rescaling according to  $H(X) = h(x)/h^\infty$  and  $X = x(3Ca)^{1/3}/h^\infty$ , one obtains the similarity equation (or Landau–Levich–Derjaguin–Bretherton (LLDB) equation)

$$H^3 H_{XXX} + 1 - H = 0, \tag{2.3}$$

which describes the transition region between the film and the caps at either end.

We begin with the front of the bubble. Starting from the film, which corresponds to the boundary condition  $H(-\infty) = 1$ , we integrate (2.3) towards  $X \rightarrow \infty$ , where the solution matches to a spherical cap of radius  $R$ , set by the tube radius. Integrating numerically, one finds that  $H_{XX}(\infty) = 0.643$ . The corresponding curvature  $h_{xx} = H_{XX}(\infty)(3Ca)^{-2/3}/h^\infty$  is thus equal to the curvature of a spherical cap,  $1/R$ , which yields Bretherton’s result (1.1), with a typical slope scale  $|dh/dx| \sim Ca^{1/3} \ll 1$ . The LLDB equation takes a single boundary condition  $H(-\infty) = 1$  (apart from translations), as a result of which a unit film thickness (1.1) is selected at the front of the bubble.

In contrast, we have to integrate in the opposite direction in the rear of the bubble: starting from the film at  $X = \infty$ , where  $H = 1$ , we now integrate towards  $X \rightarrow -\infty$ , the rear spherical cap of radius  $R$ . Here we have used the fact that the film thickness  $h^\infty$  is constant all along the middle of the bubble. Combining with (1.1), the similarity solution at the back is now determined by two boundary conditions

$$H(\infty) = 1, \tag{2.4a}$$

$$H_{XX}(-\infty) = h^\infty(3Ca)^{-2/3}/R = 0.643. \tag{2.4b}$$

Analysis of (2.3) shows that it has a unique solution subject to (2.4). While the profile has a monotonic behaviour at the front, it develops characteristic oscillations at the back.

## 2.2. Film thickness profile at the transitional state

Now we generalize the steady-state theory in the previous section to the time-dependent motion of a bubble in transition between two steady states, by imposing an instantaneous velocity change from  $U_1$  to  $U_2$ , as sketched in figure 1(a).

### 2.2.1. The uniform film regions (II and IV)

As shown in the steady problem (§ 2.1), a specific film thickness is selected near the front of the bubble based on (1.1). Thus, at the initial velocity  $U_1$ , the front of the bubble lays down a film of thickness  $h_1^\infty = 0.643(3Ca_1)^{2/3}R$ , where  $Ca_1$  is the capillary number based on  $U_1$ . After the bubble velocity is switched to  $U_2$ , this film thickness becomes  $h_2^\infty = 0.643(3Ca_2)^{2/3}R$ . We will show in the following subsection that, while the bubble front translates at speed  $U_2$ , the step connecting the two uniform film regions is effectively frozen in the laboratory frame. Taking the time of the velocity change to be  $t = 0$ , the length of region II is  $L_{II} \approx U_2 t$  (see figure 1b). In the reference frame of the bubble, the step is seen to move towards the rear. Eventually, when the step has moved past the entire bubble, a new steady state is established (figure 1a). This transitional process takes a period of time approximately  $L/U_2$ , where  $L$  is the length of the bubble.

2.2.2. *Dynamics of the step (III)*

We aim to find an approximate description for the dynamics of the step, after it has been created by an instantaneous velocity change at  $t = 0$ . We would like to know whether (i) the location of step changes in time, and whether (ii) there will be significant change in shape over the course of an experiment.

Following similar analyses in Boatto, Kadanoff & Olla (1993), McGraw *et al.* (2012), and Bäumchen *et al.* (2013), we try an ansatz in the laboratory frame, in which (2.1) holds:

$$\hat{H}(s) = \frac{h(x, t)}{h_2^\infty}, \tag{2.5a}$$

$$s = \frac{x + U_w t}{f(t)}, \tag{2.5b}$$

where  $U_w$  is the travelling wave speed of the step and  $f(t)$  describes the relaxation of the step region towards a flat state. As a result, equation (2.1) becomes

$$\frac{3\mu}{\gamma(h_2^\infty)^3} (U_w - sf_t) f^3 \hat{H}_s + (\hat{H}^3 \hat{H}_{sss})_s = 0. \tag{2.6}$$

Hence,  $U_w$  must vanish for (2.6) to be consistent, and so the step remains stationary in the frame of the tube. This result is also consistent with the physical intuition that the thin film of fluid tends to be frozen in the lab frame due to the no-slip and shear-free boundary conditions at the tube wall and the bubble surface, respectively. Thus, the step relaxation function  $f(t)$  satisfies

$$f^3 f_t = \gamma (h_2^\infty)^3 / (3\mu). \tag{2.7}$$

This means the local film profile relaxes in time according to

$$f(t) = \left( \frac{4\gamma (h_2^\infty)^3}{3\mu} t + w^4 \right)^{1/4}, \tag{2.8}$$

where  $w = f(0)^{1/4}$  represents the initial width of the step, in agreement with Bäumchen *et al.* (2013). In addition, we expect the initial step width  $w = O(R)$ . We assume that the velocity jump is triggered at  $t = 0$ , with a transition time  $\Delta t \rightarrow 0$ , and information propagates rapidly in the liquid. Therefore, the curvature of the front spherical cap can adjust to the pressure signal almost instantaneously, but bubble translation is negligible. Thus, we can relate the fluid volume in the step region to the fluid volume entering/exiting the film region due to the sudden curvature change in the front spherical cap:

$$\begin{aligned} & \pi w (R - h_1^\infty)^2 - \frac{1}{3} \pi w [(R - h_1^\infty)^2 + (R - h_2^\infty)^2 + (R - h_1^\infty)(R - h_2^\infty)] \\ & \approx \frac{2}{3} \pi [(R - h_1^\infty)^3 - (R - h_2^\infty)^3], \end{aligned} \tag{2.9}$$

where we approximate the step region of the bubble as a cone frustum on the left-hand side, and the front spherical cap as a hemisphere on the right-hand side, respectively. Assuming that  $h_1^\infty, h_2^\infty \ll R$ , the volume balance (2.9) simplifies to  $w/R \approx 3/4 = O(1)$ . This result is further confirmed in the experiments and simulations below.

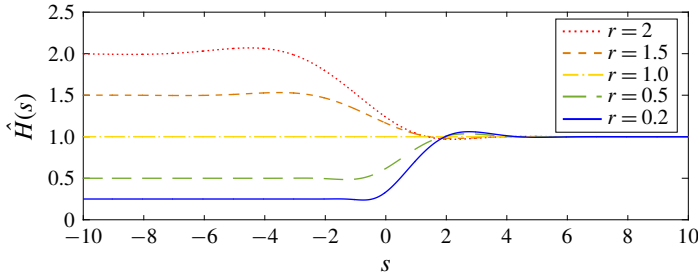


FIGURE 2. Similarity solution of the step-like region III. Results are obtained by solving (2.10) numerically for different values of  $r = h_1^\infty/h_2^\infty = [0.2, 0.5, 1, 1.5, 2]$ .

With  $s$  defined by (2.5b), the similarity equation becomes

$$(\hat{H}^3 \hat{H}_{sss})_s - s \hat{H}_s = 0, \tag{2.10}$$

with the boundary conditions  $\hat{H}(\infty) = 1$ ,  $\hat{H}(-\infty) = h_1^\infty/h_2^\infty \equiv r$  and  $\hat{H}_s(\pm\infty) = 0$ . The results corresponding to various values of  $r$  are displayed in figure 2. Similar similarity profiles in thin films have been observed in the literature (e.g. McGraw *et al.* 2012; Bäumchen *et al.* 2013), where the solutions develop small overshoots owing to the fourth-order structure of the equation.

It should be noticed that, based on the results above, the step relaxation in the transition region III is extremely slow. While the characteristic time for the translational dynamics is  $\tau_{trans} \sim L/U_2$ , the step relaxation time  $\tau_{relax}$  can be estimated using (2.8),  $\tau_{relax} \sim (\mu R/\gamma)(R/h_2^\infty)^3$ , where the initial step width  $w$  is approximated by the tube radius  $R$ . We expect to observe relaxation of the step-like profile when  $\tau_{trans} \gg \tau_{relax}$ , which in the lubrication limit requires extremely long bubbles,  $L/R \gg Ca_2^{-1}$ . Relaxation of the step is thus difficult to observe during a physical experiment, and the time duration over which a bubble transits from one steady state to another is mainly governed by the translational time scale  $\tau_{trans}$ . As a result, once the step with initial width  $w$  is formed, the film profile  $h(x, t)$  in region III translates at velocity  $-U_2$  relative to the bubble surface, similar to a propagating shock.

### 2.2.3. The front and rear similarity solutions (I and V)

Given the existence of a uniform film in region IV, we now describe how Bretherton’s theory is modified near the back of the bubble. On one hand, the entire bubble moves at the new speed  $U_2$ . On the other hand, as discussed before, the film thickness  $h_1^\infty$  is still associated with the initial speed  $U_1$ . Thus, in the reference frame of the bubble, the thin film equation is

$$h^3 h_{xxx} + Ca_2(h_1^\infty - h) = 0. \tag{2.11}$$

Next, we rescale to the LLDB equation (2.3) with the transformation  $\tilde{H} = h/h_1^\infty$  and  $\tilde{X} = x(3Ca_2)^{1/3}/h_1^\infty$ . As in the Bretherton problem, requiring the curvature of the film solution to match the curvature  $1/R$  of the rear cap, we obtain the boundary conditions

$$\tilde{H}(\infty) = 1, \tag{2.12a}$$

$$\tilde{H}_{\tilde{X}\tilde{X}}(-\infty) = h_1^\infty(3Ca_2)^{-2/3}/R. \tag{2.12b}$$



## Time-dependent motion of a confined bubble in a tube

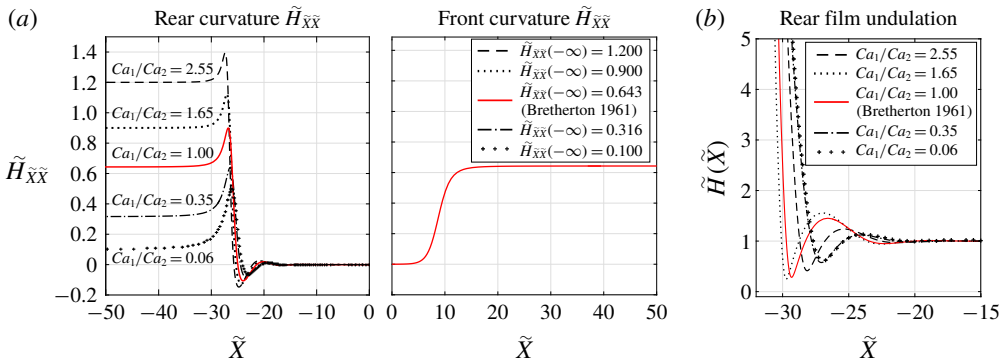


FIGURE 3. Front and rear similarity solutions. (a) The dimensionless curvatures of the similarity solution. Unlike region I, whose solution agrees with Bretherton (1961) with a dimensionless curvature  $\tilde{H}_{\tilde{X}\tilde{X}}(\infty) = 0.643$ , a family of solutions and dimensionless curvatures  $\tilde{H}_{\tilde{X}\tilde{X}}(-\infty)$  are obtained at the rear cap during the transition, depending on the ratio  $Ca_1/Ca_2$ . (b) Different film undulations  $\tilde{H}(\tilde{X})$  at the rear cap can be obtained as a result of the family of solutions.

Combining with the expression (1.1) for  $h_1^\infty$ , the dimensionless curvature for the rear spherical cap (2.12b) is simplified to

$$\tilde{H}_{\tilde{X}\tilde{X}}(-\infty) = 0.643(Ca_1/Ca_2)^{2/3}, \quad (2.13)$$

which reduces to the standard boundary condition (2.4b) when  $Ca_1 = Ca_2$ .

Our numerical results for the similarity solutions in the front and the rear of the bubble are summarized in figure 3. By construction, the rescaled curvature of the front solution always approaches the universal value of 0.643 (figure 3a). As a result, the front similarity solution is the universal solution of Bretherton. By contrast, according to (2.13) the rescaled curvature at the rear depends on the ratio of capillary numbers, producing a family of different solutions (figure 3a). With the rear spherical cap curvature varying with the ratio  $Ca_1/Ca_2$ , a small alternation to the pressure drop across the bubble rear interface may occur during the transient process. Furthermore, different film oscillations also appear on the rear air–liquid interface with various  $Ca_1/Ca_2$  ratios (figure 3b).

### 3. Experimental setup and numerical methods

Experiments are performed in a refractive index matching setup (Yu *et al.* 2017, 2018), where a  $5\times$  objective (Mitutoyo) is used in the imaging apparatus. Pure glycerol is used as the continuous phase, with viscosity  $\mu = 1.00$  Pa s (Anton Paar, Physica MCG 301) and surface tension  $\gamma = 65.4$  mN m<sup>-1</sup> (pendant drop method), respectively. A flexible tube connects the inlet of the glass capillary ( $R = 566$   $\mu$ m) to a glycerol reservoir, whose pressure is adjusted and controlled by an Elveflow<sup>®</sup> OB1 MK3 pressure and vacuum controller, with a settling time as small as 40 ms (Elveflow 2009). The pressure and flow rate are linearly correlated based on calibration. The flexible tube is partially unfilled before being inserted in the glass capillary. A single bubble is formed in the glass capillary from the air column when a positive pressure  $p_1$  is turned on. The bubble then translates at velocity  $U_1$ . The pressure

$p_2$  is switched on with a step signal when the entire bubble enters the region of interest, which triggers the transition to a new steady state at  $U_2$ . Meanwhile, the transitional dynamics of the bubble are recorded by the imaging apparatus at a film rate of 30 f.p.s.

Image processing is performed for each experimental image sequence, where a Matlab program is written to identify the boundaries of the bubble and the inner tube wall, with the error controlled within  $\pm 1$  pixel, or  $\pm 2.44 \mu\text{m}$ . The film profile  $h(x, t)$  is obtained from the difference between the position of the bubble surface and the tube wall, and the experimental bubble volume is calculated from a volume integral based on the film profile.

Numerical simulations are carried out using a commercial finite-element solver (COMSOL Multiphysics). The three-dimensional axisymmetric Stokes equations are solved numerically, and the deforming interface of the bubble is represented using the arbitrary Lagrangian–Eulerian (ALE) technique, which facilitates an accurate and sharp capture of the interface evolution. We impose a Poiseuille flow and zero pressure boundary condition at the inlet and outlet, respectively, and apply the Young–Laplace law at the bubble interface. The liquid phase is discretized and solved, assuming a zero gas–liquid viscosity ratio. The pressure on the external side of the interface is imposed by incorporating the constraint of constant bubble volume. This framework was developed by Balestra, Zhu & Gallaire (2018) and has been well validated against the classical theory (Bretherton 1961). For more details, refer to Balestra *et al.* (2018) and Hadikhani *et al.* (2018).

A slight bubble volume variation is observed in experiments when the pressure jump is applied. Therefore, two simulations using different volumes are performed: we use the volume of the initial state at  $U_1$  to obtain a steady-state bubble profile at  $Ca_1$  in the first run, and that of the transitional process in the second, where we trigger the transition to  $Ca_2$  by a sudden change of the underlying flux.

#### 4. Comparison of experiments, numerics, and analysis

The experimental and numerical results of a bubble undergoing the transitional dynamics are shown in figure 4. A typical experimental image series is shown in figure 4(a), with the zoomed-in film profiles shown in figure 4(b). The transitional motion is triggered by a pressure jump from  $p_1 = 150$  mbar to  $p_2 = 950$  mbar, corresponding to  $Ca_1 = 1.96 \times 10^{-3}$  and  $Ca_2 = 1.65 \times 10^{-2}$ , respectively. The capillary numbers are calculated from the bubble speeds, which are measured experimentally by tracking the locations of the bubble nose, determined by the intersection between the tube centreline and the front cap of the bubble surface. Time  $t = 0$  is taken as the frame right before the pressure jump is applied, and the dynamics are shown in the consecutive frames with  $\Delta t = 0.467$  s between each panel. The boundary detection results are also displayed, with the red and blue curves representing the detected bubble surface and the tube wall, respectively. As is shown in figure 4(c), the experimental (red) and numerical (blue) bubble film profiles  $h(x, t)$  are plotted in the laboratory frame within a distance  $100 \mu\text{m}$  from the tube wall. The direct comparison between experiments and simulations shows excellent agreement. The simulation results in the first run are plotted for  $t = 0$  s, and those in the second run are used for the corresponding later times. The interior of the profile has the expected structure of two uniform film regions of different thicknesses, connected by a step, which remains stationary in the laboratory frame. The film thicknesses at regions II and IV measured experimentally,  $41.5 \mu\text{m}$  and  $13.4 \mu\text{m}$ , agree well



## Time-dependent motion of a confined bubble in a tube

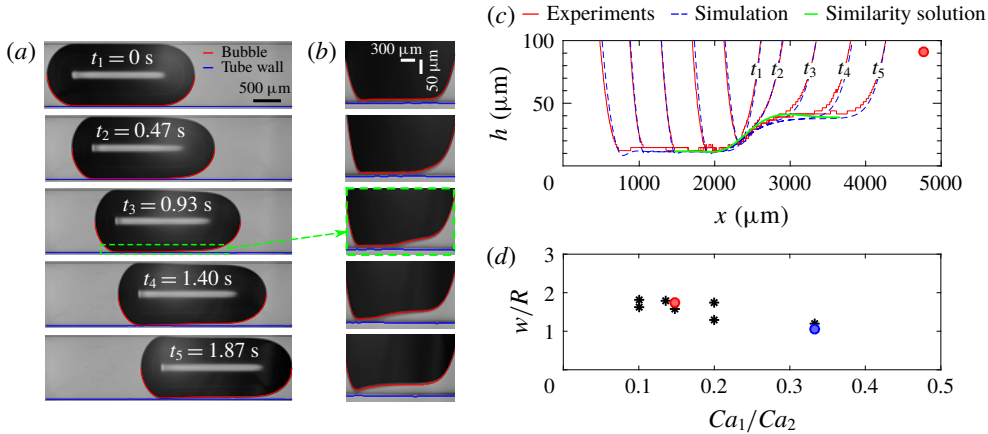


FIGURE 4. Experimental and numerical bubble profiles. (a) Experimental images and edge detection of the bubble profile. A pressure jump is applied at  $t = 0$ , which triggers the bubble to transit between steady states from  $Ca_1 = 1.96 \times 10^{-3}$  to  $Ca_2 = 1.65 \times 10^{-2}$ . The detected bubble surface and the tube wall are shown as red and blue curves, respectively. (b) Zoomed-in edge detection results in the thin film region. (c) Comparison of results in the laboratory frame among experiments (red), numerical simulations (blue) and the scaled similarity solution (2.10) (green). (d) Numerical results of the rescaled initial step width  $w/R$  at different capillary number ratios  $Ca_1/Ca_2$ . The red and blue dot symbols correspond to the cases shown in figure 4(c) and figure 5(b), respectively.

with the theoretical prediction of  $h_2^\infty$  and  $h_1^\infty$  within the experimental resolution of  $2.44 \mu\text{m}$ . In particular, note the difference between the front and rear of the bubble: while at the front the profile increases monotonically from a constant thickness towards the front cap, the behaviour at the back displays oscillations, as seen in the similarity solutions (figure 3).

The step-like region III is considered in both figure 4(c) and figure 4(d). A rapid curvature adjustment is observed prior to the step generation. In the laboratory frame (figure 4c), the lower left corner of the step is pinned while the front of the bubble moves forward at speed  $U_2$ , laying down the film to form the shape of a step. The step is seen to be stationary and not to change shape over the time scale of the experiment, which is consistent with the estimates of § 2.2.2. Based on the film thickness ratio  $r = h_1^\infty/h_2^\infty = 0.32$ , we computed the similarity solution for the step relaxation, which describes the relaxation of the step at long times, much longer than the duration of our experiment. Using the initial width  $w$  in (2.8) as an adjustable parameter, we observe that the shape of the long-time similarity solution (green) fortuitously agrees very well with the initial step (red and blue) created by the sudden change in bubble speed. We find the initial step width to be  $w = c_1 R$ , with a fitting parameter  $c_1 = 2$ . Furthermore, we repeated the numerical simulation with  $Ca_2$  ranging from  $8.6 \times 10^{-4}$  to  $2.0 \times 10^{-2}$ , and measured the step width  $w$  as the length over which the film thickness deviates from both  $h_1^\infty$  and  $h_2^\infty$  by at least 3%. As is shown in figure 4(d), the rescaled step width  $w/R = O(1)$  over different capillary number ratios  $Ca_1/Ca_2$ , which validates the order of magnitude estimate for the step width  $w$ .

To perform a quantitative test of the theory developed in § 2.2 about the front and rear caps I and V, we performed numerical simulations of a bubble at much smaller capillary numbers, for the transition from  $Ca_1 = 2.95 \times 10^{-4}$  to  $Ca_2 = 8.57 \times 10^{-4}$ ,

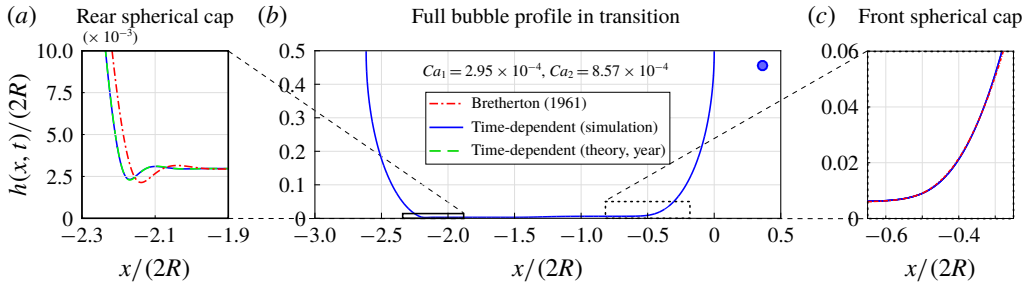


FIGURE 5. Direct comparison for the front and rear spherical caps between the numerical simulation results (blue), and theoretical results both from § 2.2 (green) and Bretherton (1961) (red). The bubble is undergoing transition from one speed to another, and the profile at simulation time  $t = 0.88$  is shown. (b) The results are rescaled by the tube diameter  $2R$  and plotted from the tube wall to the tube centreline. (a) Zoomed-in view near the rear spherical cap, where the results from the simulation and time-dependent theory agree, but both deviate from the classic steady-state theory at  $Ca_1$ . (c) Enlarged region near the front spherical cap, where the simulation results agree with the classic steady-state theory at  $Ca_2$ .

as shown in figure 5. The profile of the entire bubble, obtained from the numerical simulation, is plotted in figure 5(b). In order to compare with the theory, the zoomed-in views of the rear and front similarity regions are displayed in panels (a) and (c), respectively. Starting in the front (figure 5c), excellent agreement is shown between the numerical simulation (blue) and the theoretical similarity solution at  $Ca_2$  (red), rescaled according to § 2.1. As explained before, the bubble front profile is identical to that of Bretherton’s steady-state theory. The rear region is shown in figure 5(a), comparing the numerical simulation (blue) to the time-dependent theory (green) with  $Ca_1/Ca_2 = 0.35$ , where the results agree so well as to be nearly indistinguishable. The time-dependent similarity solution is rescaled based on § 2.2.3, and is one of the solutions shown in figure 3. For comparison, as the red curve, we also show the shape one would have obtained from the steady theory. This demonstrates that the unsteadiness introduces a significant change in the shape of the rear film.

### 5. Concluding remarks

Theoretical predictions are given for the time-dependent film profile of a confined bubble transitioning between two steady states, triggered by an instantaneous velocity change. The theory is validated with experiments and numerical simulations. Several film regions can be categorized during the transition, as shown in figure 1(b). The film profile near the front cap (I) and the thickness of the front uniform film region (II) are identical to those at the second steady state, with the length of region II extending in time. The rear uniform film region (IV) is of constant thickness  $h_1^\infty$ , identical to that at the initial steady state. The two uniform film regions II and IV are connected by a step-like film region (III), which is stationary in the laboratory frame. A similarity solution is obtained for the film profile at region III. However, for the range of capillary numbers studied, the step relaxation is too slow to be observed in the experiments and simulations. During the transition, the rear film solution (V) is modified according to the ratio  $Ca_1/Ca_2$ . This modification not only provides a family of solutions near the rear spherical cap (figure 3), but it also modifies the undulations

at the rear transitional region near the spherical cap (figure 5). It has not escaped our notice that the present unsteady theory can be generalized to continuously varying bubble speeds, as well as continuously varying tube cross-sections. A fuller account of these cases is currently under preparation.

## Acknowledgements

We thank the NSF for support via grant CBET-1804863. J.E. acknowledges support from the Leverhulme Trust through International Academic Fellowship IAF-2017-010. L.Z. thanks the Swedish Research Council for a VR International Postdoc grant 2015-06334. Y.E.Y. acknowledges support from Princeton Environmental Institute through the Mary and Randall Hack '69 Research Fund.

## References

- ATASI, O., KHODAPARAST, S., SCHEID, B. & STONE, H. A. 2017 Effect of buoyancy on the motion of long bubbles in horizontal tubes. *Phys. Rev. Fluids* **2** (9), 094304.
- AUSSILLOUS, P. & QUÉRÉ, D. 2000 Quick deposition of a fluid on the wall of a tube. *Phys. Fluids* **12** (10), 2367–2371.
- BALESTRA, G., ZHU, L. & GALLAIRE, F. 2018 Viscous Taylor droplets in axisymmetric and planar tubes: from Bretherton's theory to empirical models. *Microfluid. Nanofluid.* **22** (6), 67.
- BÄUMCHEN, O., BENZAQUEN, M., SALEZ, T., MCGRAW, J. D., BACKHOLM, M., FOWLER, P., RAPHAËL, E. & DALNOKI-VERESS, K. 2013 Relaxation and intermediate asymptotics of a rectangular trench in a viscous film. *Phys. Rev. E* **88**, 035001.
- BLUNT, M. J. 2001 Flow in porous media pore-network models and multiphase flow. *Curr. Opin. Colloid Interface Sci.* **6** (3), 197–207.
- BOATTO, S., KADANOFF, L. P. & OLLA, P. 1993 Traveling-wave solutions to thin-film equations. *Phys. Rev. E* **48**, 4423–4431.
- BRETHERTON, F. P. 1961 The motion of long bubbles in tubes. *J. Fluid Mech.* **10** (02), 166–188.
- EGGERS, J. & FONTELOS, M. A. 2015 *Singularities: Formation, Structure, and Propagation*. Cambridge University Press.
- ELVEFLOW 2009 Responsiveness of OB1 piezo-electric technologies. <https://www.elflow.com/microfluidic-tutorials/microfluidic-reviews-and-tutorials/responsiveness-of-flow-control-instruments>.
- FAIRBROTHER, F. & STUBBS, A. E. 1935 119. Studies in electro-endosmosis. Part VI. The 'bubble-tube' method of measurement. *J. Chem. Soc.* **1**, 527–529.
- GAVER, D. P., HALPERN, D., JENSEN, O. E. & GROTBORG, J. B. 1996 The steady motion of a semi-infinite bubble through a flexible-walled channel. *J. Fluid Mech.* **319**, 25–65.
- HADIKHANI, P., HASHEMI, S. M. H., BALESTRA, G., ZHU, L., MODESTINO, M. A., GALLAIRE, F. & PSALTIS, D. 2018 Inertial manipulation of bubbles in rectangular microfluidic channels. *Lab on a Chip* **18** (7), 1035–1046.
- HAZEL, A. L. & HEIL, M. 2003 Three-dimensional airway reopening: the steady propagation of a semi-infinite bubble into a buckled elastic tube. *J. Fluid Mech.* **478**, 47–70.
- HEIL, M. 2001 Finite Reynolds number effects in the Bretherton problem. *Phys. Fluids* **13** (9), 2517–2521.
- KHODAPARAST, S., MAGNINI, M., BORHANI, N. & THOME, J. R. 2015 Dynamics of isolated confined air bubbles in liquid flows through circular microchannels: an experimental and numerical study. *Microfluid. Nanofluid.* **19** (1), 209–234.
- KOTULA, A. P. & ANNA, S. L. 2012 Probing timescales for colloidal particle adsorption using slug bubbles in rectangular microchannels. *Soft Matt.* **8** (41), 10759–10772.
- LAMSTAES, C. & EGGERS, J. 2017 Arrested bubble rise in a narrow tube. *J. Stat. Phys.* **167** (3–4), 656–682.
- LEUNG, S. S. Y., GUPTA, R., FLETCHER, D. F. & HAYNES, B. S. 2012 Gravitational effect on Taylor flow in horizontal microchannels. *Chem. Engng Sci.* **69** (1), 553–564.

- MAGNINI, M., FERRARI, A., THOME, J. R. & STONE, H. A. 2017 Undulations on the surface of elongated bubbles in confined gas–liquid flows. *Phys. Rev. Fluids* **2** (8), 084001.
- MCGRAW, J. D., SALEZ, T., BÄUMCHEN, O., RAPHAËL, E. & DALNOKI-VERESS, K. 2012 Self-similarity and energy dissipation in stepped polymer films. *Phys. Rev. Lett.* **109** (12), 128303.
- OLGAC, U. & MURADOGLU, M. 2013 Effects of surfactant on liquid film thickness in the Bretherton problem. *Intl J. Multiphase Flow* **48**, 58–70.
- PARK, C. W. 1992 Influence of soluble surfactants on the motion of a finite bubble in a capillary tube. *Phys. Fluids A* **4** (11), 2335–2347.
- QUÉRÉ, D. 1999 Fluid coating on a fiber. *Annu. Rev. Fluid Mech.* **31** (1), 347–384.
- RATULOWSKI, J. & CHANG, H. C. 1990 Marangoni effects of trace impurities on the motion of long gas bubbles in capillaries. *J. Fluid Mech.* **210**, 303–328.
- DE RYCK, A. 2002 The effect of weak inertia on the emptying of a tube. *Phys. Fluids* **14** (7), 2102–2108.
- STEBE, K. J. & BARTHES-BIESEL, D. 1995 Marangoni effects of adsorption–desorption controlled surfactants on the leading end of an infinitely long bubble in a capillary. *J. Fluid Mech.* **286**, 25–48.
- STONE, H. A. 2010 Interfaces: in fluid mechanics and across disciplines. *J. Fluid Mech.* **645**, 1–25.
- TAYLOR, G. I. 1961 Deposition of a viscous fluid on the wall of a tube. *J. Fluid Mech.* **10** (02), 161–165.
- YU, Y. E., KHODAPARAST, S. & STONE, H. A. 2017 Armoring confined bubbles in the flow of colloidal suspensions. *Soft Matt.* **13** (15), 2857–2865.
- YU, Y. E., KHODAPARAST, S. & STONE, H. A. 2018 Separation of particles by size from a suspension using the motion of a confined bubble. *Appl. Phys. Lett.* **112** (18), 181604.